Chinese Journal of Catalysis 35 (2014) 2029–2037

available at www.sciencedirect.com

ScienceDirect

journal homepage: www.elsevier.com/locate/chnjc

Article

Microwave-assisted fast fabrication of a nanosized Pt_3Co alloy on reduced graphene oxides

Juanjuan Shi, Renfeng Nie, Mengyuan Zhang, Mengsi Zhao, Zhaoyin Hou *

Institute of Catalysis, Department of Chemistry, Zhejiang University, Hangzhou 310028, Zhejiang, China

ARTICLE INFO

Article history:
Received 30 July 2014
Accepted 30 September 2014
Published 20 December 2014

Keywords:
graphene
Pt_3Co
microwave irradiation
cinnamaldehyde
hydrogenation

ABSTRACT

Ultrafine and homogenously dispersed Pt_3Co alloy nanoparticles were fabricated on reduced graphene oxide (RGO) in a few minutes under microwave irradiation. Characterization results confirmed that microwave irradiation was important for higher metal utilization, the easy control of alloy composition, improved dispersion of the Pt_3Co particles and minimizing the re-graphitization of the parent RGO by comparison with conventional solvent-thermal and impregnation methods. This Pt_3Co/RGO-MW catalyst was extremely active and selective during the hydrogenation of cinnamaldehyde to cinnamyl alcohol. The calculated specific activity of each Pt atom in the Pt_3Co/RGO-MW at 70 °C was 23.8 min^{-1}.

1. Introduction

Nanosized metal particles have been extensively exploited for potential application in catalysis, sensors and biosensors, electro-oxidation, energy conversion devices, and the production of hydrogen because of their unique physicochemical properties. These nanostructures have allowed new insights into traditional catalysis and many achievements have been reported in recent years [1,2].

Nanosized Pt and Pt-alloys have been extensively investigated because of their excellent catalytic performance in fuel cells [3,4], selective oxidation [5–7], and in the selective hydrogenation of unsaturated aldehydes [8–10]. Pt-alloys can reduce the amount of expensive Pt required and some have enhanced activity compared with monometallic Pt. The Pt_3Co alloy shows remarkable activity in electro-catalytic oxygen reduction in fuel cells [11–14], and the selective hydrogenation of α,β-unsaturated aldehydes [15,16]. However, the controlled synthesis of nanosized Pt-alloys is a challenge in terms of controlling the particle size, size distribution and metal composition. Most reported methods employ surfactants to control the Pt-alloy particle size [15–18]. However, for catalytic application, it is more desirable to synthesize uncapped particles that exhibit similar or higher stability compared with their capped counterparts [19]. Several methods such as co-precipitation [20], impregnation [6,7], and surface organometallic reactions [21] have been reported. However, these processes are time-consuming and generate waste solvents while high temperatures and pressures are required to alloy different metal components. Among the reported methods, impregnation is simple and the loading efficiency of metal precursors is low. A Pt-Co alloy that was prepared by a precipitation method was found to agglomerate easily and had a varied Pt-Co alloy composition [22].

---

* Corresponding author. Tel/Fax: +86-571-88273283; E–mail: zyhou@zju.edu.cn

This work was supported by the National Natural Science Foundation of China (21473155, 21273198, 21073159) and the Natural Science Foundation of Zhejiang Province (L12B03001).

DOI: 10.1016/S1872-2067(14)60232-1 | http://www.sciencedirect.com/science/journal/18722067 | Chin. J. Catal., Vol. 35, No. 12, December 2014

Graphene possesses a high surface area that is useful for the dispersion of metal nanoparticles (NPs) and its micropore-free structure contains one or a few sheet layers, which is useful for the transfer of reactants and products. Good electrical conductivity is required for electron transfer in catalysis and graphene is thought to have high chemical reactivity [23–28]. However, graphene is prone to aggregation during drying and graphite may form in these prepared catalysts because of van der Waals interactions [29,30].

Microwave irradiation, as a rapid, uniform and effective heating method, has received considerable attention as a new, promising method to weaken the formation of "re-graphitized" carbon regions of graphene [25,31]. Microwave irradiation-assisted reduction has also been proposed for the controlled synthesis of Pt-based electro-catalysts [32–34]. Knupp et al. [32] reported that uniformly dispersed Pt NPs with a high loading efficiency could be deposited on carbon nanotubes and carbon nanofibers using microwave irradiation-assisted heating techniques. Yu et al. [34] found that polymer-stabilized platinum colloids with a near-uniform spherical shape (narrow size of 2–4 nm) could be prepared by microwave dielectric heating.

In this work, we report a microwave irradiation-assisted and fast synthesis routine for the production of an ultrafine and homogenously dispersed Pt_3Co alloy on the surface of reduced graphene oxide (Pt_3Co/RGO-MW). The synthesized Pt_3Co/RGO-MW was compared with samples prepared by impregnation (Pt_3Co/RGO-IM) and conventional solvent-thermal (Pt-Co/RGO-ST) methods. The performance of these catalysts in the chemoselective hydrogenation of *α,β*-unsaturated aldehydes (cinnamaldehyde, CAL) to their corresponding unsaturated alcohols (cinnamyl alcohol, COL) is discussed.

2. Experimental

2.1. Catalyst preparation

Synthesis of the Pt_3Co/RGO-MW catalyst. Graphene oxide (GO) was prepared by a modified Hummers method [35]. Pt-Co alloyed NPs with a Pt/Co molar ratio of 3:1 on RGO sheets were synthesized as follows: GO (0.10 g C) was added to a solution of ethylene glycol (EG, 100 mL) and this solution was sonicated for 30 min to obtain a homogenous liquid GO suspension. Weighed amounts of H_2PtCl_6 and $Co(CH_3COO)_2$ at a Pt/Co molar ratio of 3:1 were added to the suspension and it was stirred for 2 h. The pH of the above mentioned suspension was adjusted to 11–12 using a NaOH/EG solution. This solution was subjected to microwave heating for 7.5 min in a microwave oven (Sineo, MAS-II, 600 W, 2.45 GHz) operated at 145 °C. After microwave irradiation, the suspension was cooled to room temperature and the solid product was isolated and washed with distilled water until it was free of Cl^-. It was then dried in a vacuum oven at 40 °C for 10 h. This catalyst was designated Pt_3Co/RGO-MW. Monometallic Pt/RGO-MW and Co/RGO-MW were also prepared in a similar manner. The Pt and Co content of the prepared catalysts were determined by inductively coupled plasma-atomic emission spectroscopy (ICP, Plasma Spec II spectrometer).

Synthesis of the Pt_3Co/RGO-IM catalyst. As a reference, Pt-Co alloyed NPs on RGO were also prepared by the impregnation method [22] and the product was designated Pt_3Co/RGO-IM. Weighed amounts of H_2PtCl_6 and $Co(CH_3COO)_2$ with a Pt/Co molar ratio of 3:1 were added to an aqueous solution of GO (100 mL). The solution of GO and metal ions was magnetically stirred overnight. Finally, 50 mL of $NaBH_4$ solution (20 mmol/L) was added dropwise to the solution. After continuously stirring for 24 h, the resulting solution was filtered and washed until it was free of Cl^-. It was then dried in a vacuum oven at 40 °C for 10 h.

Synthesis of the Pt-Co/RGO-ST catalyst. A conventional solvent-thermal method was used, as previously reported [9]. The produced catalyst was designated Pt-Co/RGO-ST. The prepared GO (0.10 g C) was added to a solution containing EG (100 mL) and this solution was sonicated for 30 min to obtain a liquid suspension of GO. H_2PtCl_6 and $Co(CH_3COO)_2$ at a Pt/Co molar ratio of 3:1 were then added. This mixture was further stirred for 2 h to fully exfoliate the GO. Subsequently, the pH of the above-mentioned suspension was adjusted to 11–12 using a NaOH/EG solution. The mixture was then transferred to a stainless steel autoclave with a Teflon inner layer and put into an oil bath at 145 °C for 24 h under constant stirring. The formed catalyst was separated by filtration and washed with ethanol until it was free of Cl^-. It was then dried in a vacuum oven at 40 °C for 10 h.

2.2. Characterization

X-ray diffraction (XRD) patterns were recorded on a diffractometer (RIGAKUD/MAX 255/PC) at 40 kV and 100 mA with Cu K_α radiation (λ = 0.15406 nm). The crystallite size of Pt or the Pt-Co alloy was calculated using the Scherrer equation. Raman spectra were collected on a Rhenishaw 2000 Confocal Raman Microprobe (Rhenishaw Instruments, UK) using a 514.5 nm argon laser. Tapping mode atomic force microscopy (AFM) measurements were performed using a multimode scanning probe microscope (SPM) from Digital Instruments with a Nanoscope IIIa controller. Scanning transmission electron microscopy (STEM) and high-angle annular dark field (HAADF) imaging were used to observe individual particles at atomic resolution with an aberration corrected JEOL 2200FS (S)TEM operating at 200 kV. X-ray energy dispersive spectrometer (EDS) spectra of individual particles larger than 1–2 nm were obtained. Pt, Co, and the Pt-Co alloy were identified using fast Fourier transform (FFT) high-resolution TEM analysis. X-ray photoelectron spectra (XPS) were recorded on a Perkin-Elmer PHI ESCA System. The X-ray source was a Mg standard anode (1253.6 eV) operated at 12 kV and 300 W.

2.3. Catalytic reactions

The selective hydrogenation of CAL was performed in a 100 mL stainless steel autoclave with a Teflon inner layer. In a typical procedure, the catalyst was first dispersed in 20.0 mL ethanol, and then 8.0 mmol CAL was added while stirring. After sealing the reactor, the air content was quickly purged by flushing three times with 2.0 MPa H_2. The autoclave was then heated to 70 °C and the reaction mixture was stirred (at 1000 rpm) with a magnetic stirrer (MAG-NEO, RV-06M, Japan). After the reaction, the solid catalyst was separated by centrifugation and the products were analyzed by gas chromatography (HP 5890, USA) using a 30 m capillary column (HP-5) and a flame ionization detector. All the products were confirmed by GC-MS (Agilent 6890-5973N).

3. Results and discussion

3.1. Structural characterization

The Pt and Co content of the prepared Pt-Co/RGO catalysts were determined by ICP and are summarized in Table 1. We found that the composition of the prepared Pt_3Co/RGO-MW fits the controlled value well. The utilization efficiency of the Pt precursor was as high as 98.1%, and the Pt/Co molar ratio was 3:1.02. This fits the control level (3:1) well. The utilization efficiency of the Pt precursor was low in the samples prepared by the impregnation (77.8%, in Pt_3Co/RGO-IM) and conventional solvent-thermal (89.2%, in Pt-Co/RGO-ST) methods. The calculated Pt/Co molar ratio changed to 3:1.05 and 3:0.35, respectively. These data indicate that microwave irradiation is an important method for the fabrication of bimetallic catalysts on the surface of RGO. This method is characterized by short reaction time, high Pt and Co precursor utilization and the easy control of sample molar ratio.

XRD patterns of the Pt-Co/RGO catalysts prepared using the different methods are shown in Fig. 1. The presence of metallic Pt in Pt/RGO-MW is indicated by the characteristic (111), (200), and (220) plane diffraction peaks of Pt at 2θ = 39.8°, 46.3°, and 67.5°, respectively (JCPDS 04-0802). Three distinct peaks at 2θ = 40.5°, 47.1°, and 68.8° were found for Pt_3Co/RGO-MW. These fit the (111), (200), and (220) planes of the Pt_3Co alloy well (JCPDS 29-0499), respectively [36]. From the broadening of the (220) plane, the calculated crystallite size of these alloy particles is 2.1 nm (summarized in Table 1). These diffraction peaks were sharp in the pattern of Pt-Co/RGO-ST and Pt_3Co/RGO-IM. This behavior can be attributed to the uneven dispersion of the alloyed NPs. The calculated crystallite size of the alloyed NPs increased to 5.3 nm and 10.6 nm, respectively. Since no separate Co or Co oxide peaks are present in Fig. 1(2)–(4), the Pt-Co alloy mainly formed in the bimetallic catalysts.

Table 1
Metal loading and dispersion on RGO.

Catalyst	Metal content [a] (%)		Utilization of Pt [b] (%)	Particle size (nm)	
	Pt	Co		XRD	TEM
Co/RGO-MW	—	1.6	—	—	—
Pt/RGO-MW	15.5	—	98.1	2.4	2.5
Pt_3Co/RGO-MW	15.5	1.6	98.1	2.1	2.3
Pt_3Co/RGO-IM	12.3	1.3	77.8	10.6	11.6
Pt-Co/RGO-ST	14.1	0.5	89.2	5.3	5.4

[a] The controlled Pt and Co loading amounts were 15.8 and 1.6 mass percent with respect to C, respectively.

[b] The utilization of Pt was calculated as: real loading amount of Pt in the prepared catalysts/the amount of added Pt.

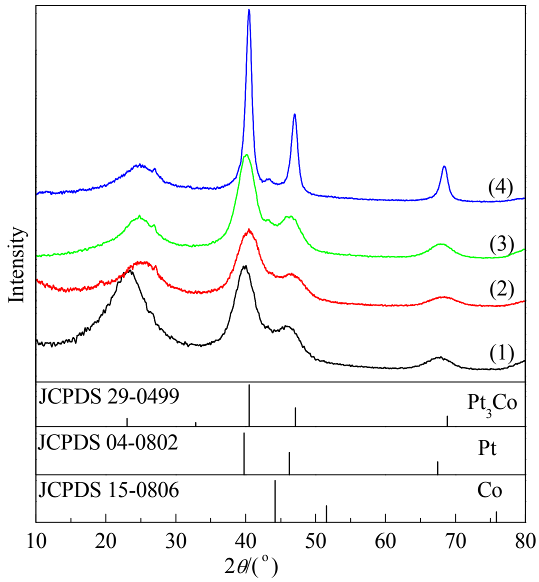

Fig. 1. XRD patterns of Pt/RGO-MW (1), Pt_3Co/RGO-MW (2), Pt-Co/RGO-ST (3), and Pt_3Co/RGO-IM (4).

A broad peak between 2θ = 17° and 30° is present in the patterns of all the samples and this is assigned to the characteristic structure of RGO wherein the formation of "re-graphitized" carbon regions and disordered restacking occurred because of van der Waals attractive interactions [23]. By comparison with Pt_3Co/RGO-IM and Pt-Co/RGO-ST, this Pt_3Co/RGO-MW diffraction peak was broader, indicating the relatively less dense and well-exfoliated state of the graphene sheets.

Raman spectra of the RGO-supported Pt-Co catalysts are shown in Fig. 2. The D band of these catalysts is present at ~1350 cm^{-1} and it is associated with the defect-related A_{1g} mode [37–39]. The G band at ~1580 cm^{-1} represents a first-order scattering of the E_{2g} vibrational state with the graphitic hexagon-pinch mode. The calculated R (I_D/I_G) intensity

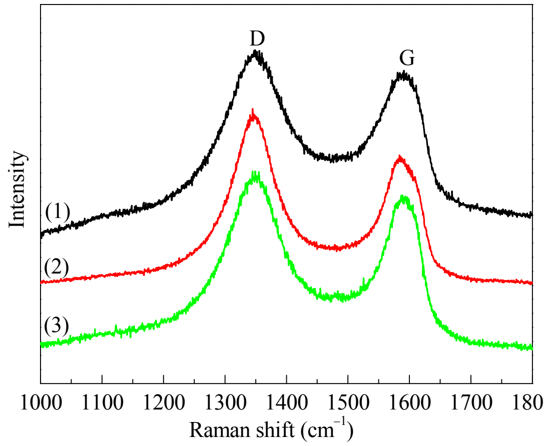

Fig. 2. Raman spectra of Pt_3Co/RGO-IM (1), Pt-Co/RGO-ST (2), and Pt_3Co/RGO-MW (3).

ratios of Pt_3Co/RGO-IM (Fig. 2(1)), Pt-Co/RGO-ST (Fig. 2(2)), and Pt_3Co/RGO-MW (Fig. 2(3)) were 1.37, 1.17, and 1.05, respectively. These results show that microwave irradiation is effective in reducing GO and it subsequently results in the restoration of the *sp*^{2} network with small and isolated aromatic domains within the sheets by comparison with conventional synthetic methods.

The thickness of the RGO support in these prepared catalysts was measured by AFM, and representative images are shown in Fig. 3. The apparent height of the microwave-treated RGO-MW sheets between the two red marks was 0.725 nm (Fig. 3(a)), and this was expected to be thinner than that of GO (typical thickness of about 0.8 nm) because of the removal of covalently bound oxygen and the resumption of aromatic or conjugated systems [38]. This thickness indicates that microwave-treated RGO-MW contains about two sheets because the ideal thickness of a graphene plane is 0.335 nm [40]. However, the distances between the closest RGO sheets prepared by the conventional synthetic methods were 1.291 (in RGO-IM, Fig. 3(b)) and 1.933 nm (in RGO-ST, Fig. 3(c)) for four and six graphene layers, respectively. These data further confirm that microwave irradiation can weaken the “re-graphitization” of exfoliated GO during the reduction of metal salts.

Typical TEM images and the corresponding particle size distributions of the Pt_3Co/RGO-MW, Pt_3Co/RGO-IM and Pt-Co/RGO-ST catalysts are given in Fig. 4. A large amount of ultrafine, highly dispersed Pt_3Co NPs of 1–5 nm in size (with an average diameter of 2.3 nm) were present in the TEM and STEM images of Pt_3Co/RGO-MW (Fig. 4(a)–(d)). The HRTEM images and a FFT (Fig. 4(c), (d)) analysis of representative Pt-Co particles show the formation of a uniform Pt_3Co alloy with predominant (111) and (200) planes. HAADF (Fig. 4(e), (f)) images of single Pt_3Co NPs show that good spatial correspondence exists in the Co and Pt elemental maps which are

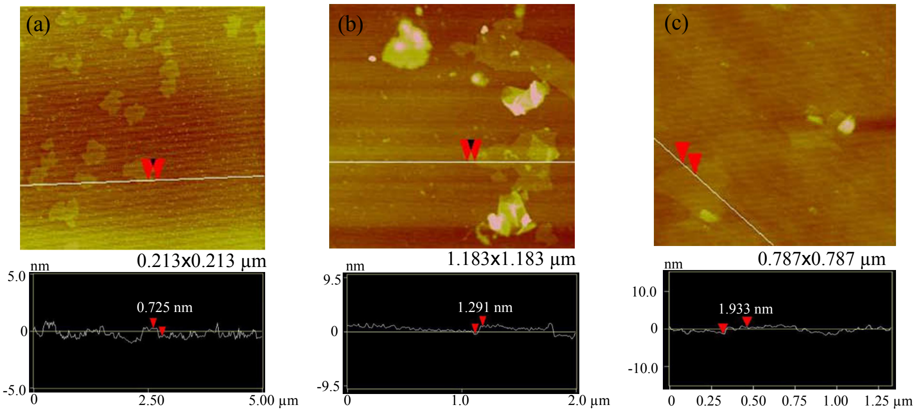

Fig. 3. AFM images and section analysis of RGO-MW (a), RGO-IM (b), and RGO-ST (c).

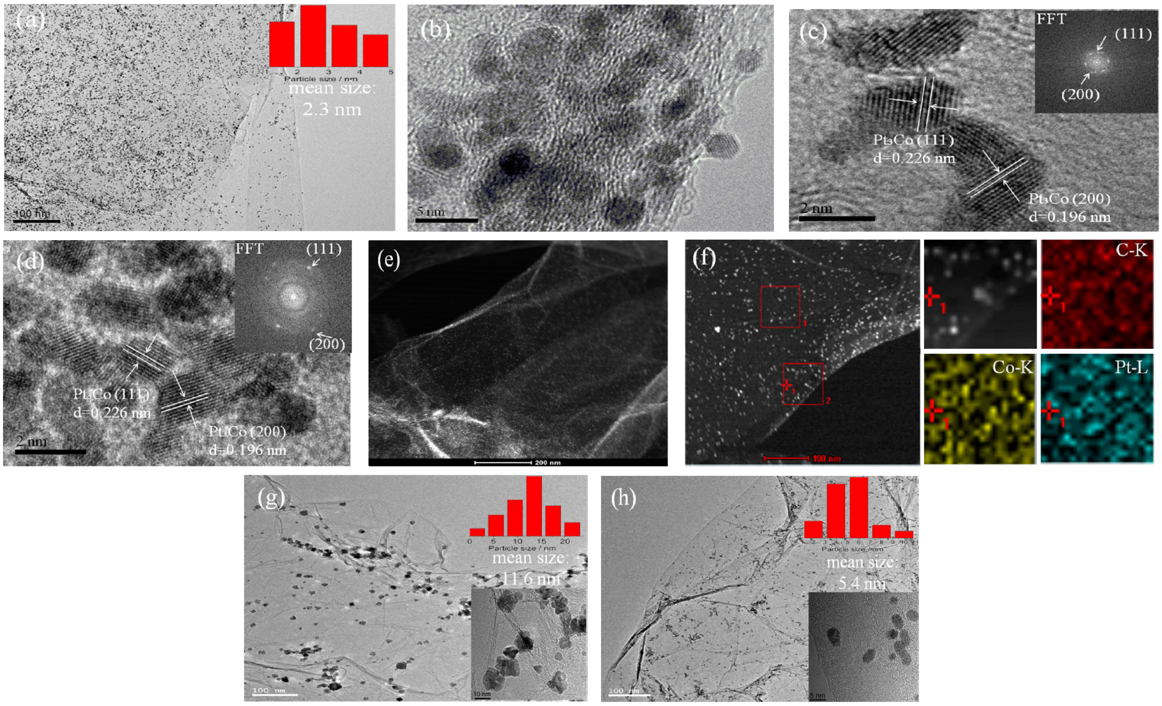

Fig. 4. (HR)TEM (a)–(d) images of Pt_3Co/RGO-MW, and its corresponding FFT (inset (c),(d)); (e),(f) HAADF-STEM images and elemental maps for Pt and Co metals of Pt_3Co/RGO-MW; (g) HRTEM images of Pt_3Co/RGO-IM and (h) Pt-Co/RGO-ST catalysts.

determined by the intensity of their K and L lines, respectively. On the other hand, big Pt_3Co clusters with an average diameter of 11.6 nm formed in Pt_3Co/RGO-IM (Fig. 4(g)). The Pt-Co alloy NPs dispersed unevenly in Pt-Co/RGO-ST (Fig. 4(h)) and the detected Pt-Co particles were 1–11 nm in size (with an average diameter of 5.4 nm). These results further confirm that microwave irradiation is an important method for the fabrication of an ultrafine, homogenously dispersed Pt_3Co alloy on the surface of RGO.

Fig. 5 shows C1*s* XPS spectra of GO, Pt_3Co/RGO-MW, Pt_3Co/RGO-IM and Pt-Co/RGO-ST. Four kinds of carbon specie carbon in the main frame (C–C, sp^2) at 284.6 eV, carbon with dangling OH groups or an epoxy linkage (C–OH/epoxy) at 286.6 eV, carbonyls (C=O) at 287.7 eV and carboxylates (O–C=O) at 289.0 eV [18,24] were detected in these samples. The ratios of these carbon species in the GO and the prepared catalysts were deconvoluted and are summarized in Table 2. The heterocarbon group content (C–O, C=O, and O–C=O) decreased dramatically from 60.7% (in GO, Fig. 5(a)) to 17.1% (in Pt_3Co/RGO-MW, Fig. 5(b)). This indicates that many oxygen functional groups were partially removed during the reduction process. The heterocarbon components of Pt_3Co/RGO-IM (Fig. 5(c)) and Pt-Co/RGO-ST (Fig. 5(d)) were also reduced to 21.1% and 24.0%, respectively.

The Pt 4*f* XPS spectra of the Pt_3Co/RGO-MW, Pt_3Co/RGO-IM and Pt-Co/RGO-ST catalysts are shown in Fig. 6. The most intense doublet with binding energy of 71.4 eV and 74.8 eV is attributed to metallic Pt(0). The peaks at 72.4 eV and 75.8 eV are attributed to Pt(II) in either PtO or $Pt(OH)_2$ [24,41,42]. It is interesting to note that the Pt(0) content of Pt_3Co/RGO-MW and Pt_3Co/RGO-IM (80.3% and 79.8%, respectively) is higher than that of Pt-Co/RGO-ST (75.8%). This might come from the formation of the Pt_3Co alloy that depresses the oxidation of Pt by air or oxygen in the RGO (Fig. 6(a), (b), Table 2). The Co 2*p* features consist of two main peaks of $2p_{3/2}$ and $2p_{1/2}$ at 780 eV and 797 eV, respectively, and these are assigned to Co(II). Additional satellites centered at 786 eV and 804 eV also confirmed the formation of Co(II) [43]. The shoulder peak at 778 eV indicated the presence of Co(0) and its intensity was weak because Co is a more oxophilic metal compared with Pt and would show an oxidation effect much more readily [44].

3.2. *Catalytic activity during the hydrogenation of CAL*

The selective hydrogenation of *α*,*β*-unsaturated aldehydes to their corresponding unsaturated alcohols is of great importance in the production of fine chemicals and pharmaceutical intermediates. This reaction was also studied in detail to

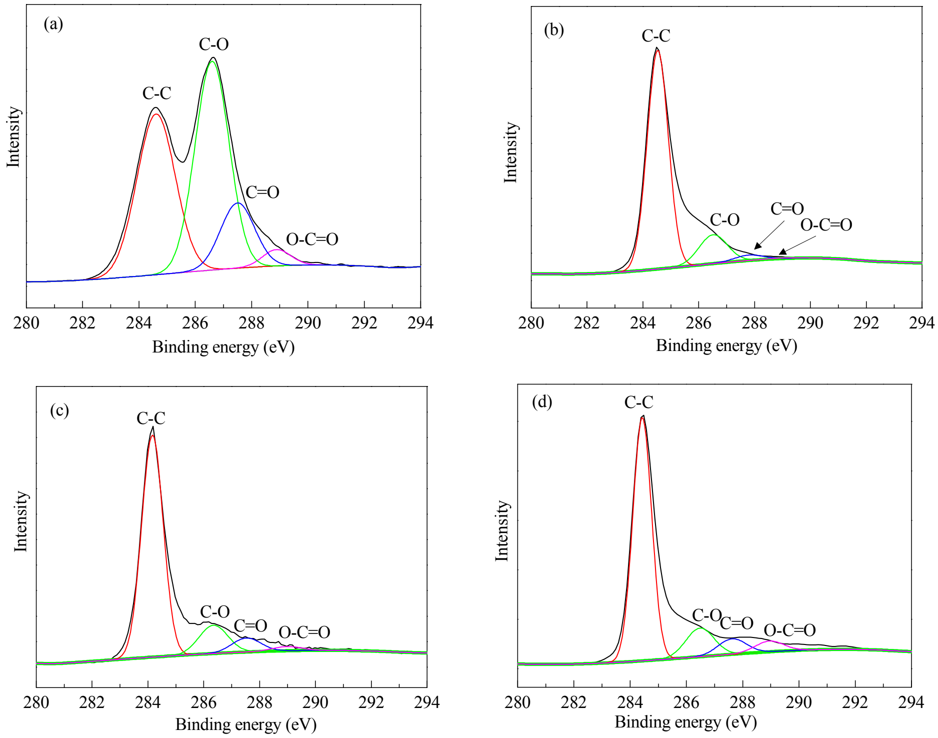

Fig. 5. C1*s* XPS spectra of GO (a), Pt_3Co/RGO-MW (b), Pt_3Co/RGO-IM (c), and Pt-Co/RGO-ST (d).

Table 2
Distribution of functional groups from the XPS data.

Catalyst	Relative atomic content (%)				Heterocarbon Component (%)	Relative atomic content (%)	
	C–C	C–O	C =O	O =C–O		Pt(0)	Pt(II)
GO	39.3	40.7	15.2	4.8	60.7	—	—
Pt_3Co/RGO-MW	82.9	14.1	2.7	0.3	17.1	80.3	19.7
Pt_3Co/RGO-IM	78.9	12.8	6.3	2.0	21.1	79.8	20.2
Pt-Co/RGO-ST	76.0	12.6	6.8	4.6	24.0	75.8	24.2

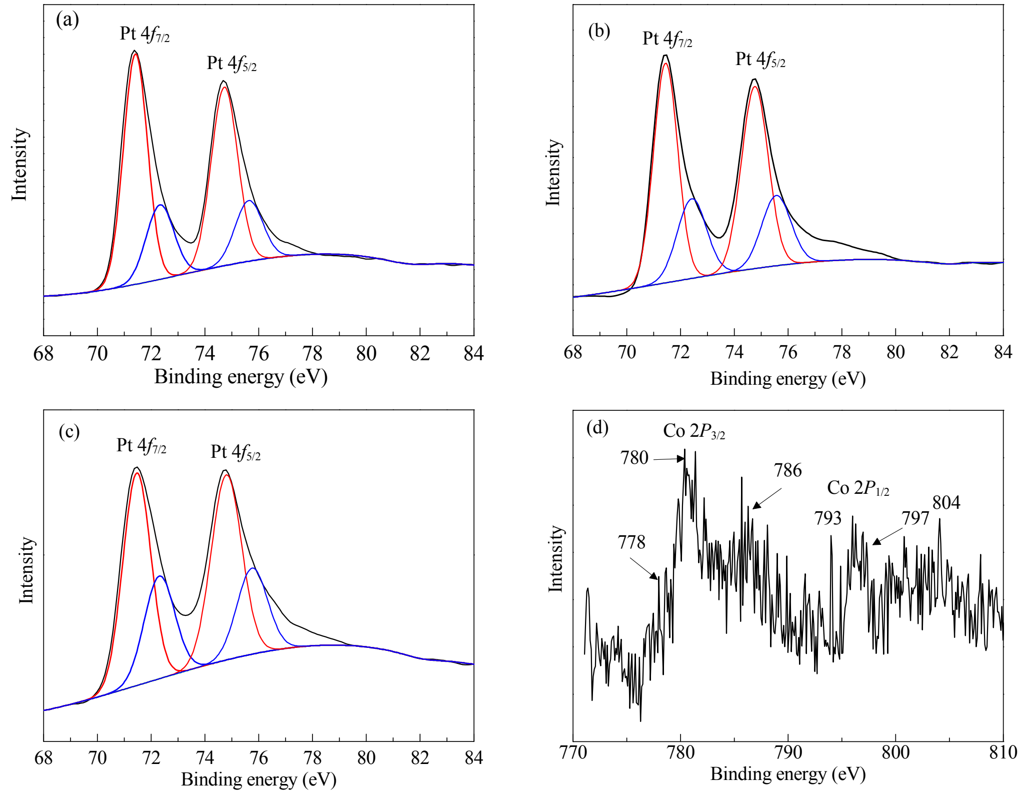

Fig. 6. XPS spectra of Pt 4*f* in Pt_3Co/RGO-MW (a), Pt_3Co/RGO-IM (b), Pt-Co/RGO-ST (c) (Pt(0) in red, Pt(II) in blue), and Co 2*p* spectra for Pt_3Co/RGO-MW (d).

probe the selective activation of C=C or C=O bonds [8–10,15,16]. In this work, the selective hydrogenation of CAL was carried out as a model reaction for the prepared Pt-Co/RGO, and the results are summarized in Table 3. Under the reaction conditions used (CAL/Pt (substrate/catalyst, S/C) molar ratio = 1127, 70 °C, 2.0 MPa), the main product was found to be COL, and the byproducts were hydrocinnamaldehyde (HCAL) and hydrocinnamyl alcohol (HCOL). Pure RGO-MW and Co/RGO-MW were inactive during the reaction (entries 1 and 2). A significant conversion of CAL was apparent over Pt/RGO-MW, Pt_3Co/RGO-MW, Pt_3Co/RGO-IM and Pt-Co/RGO-ST (entries 3–6). The conversion of CAL over Pt/RGO-MW and Pt_3Co/RGO-MW at 90 min was 92.6% and 99.7%, respectively. However, the selectivity toward COL over Pt_3Co/RGO-MW (95.3%) was obviously higher than that over Pt/RGO-MW (42.1%). The selectivity of COL toward Pt_3Co/RGO-IM (92.2%, entry 5) and Pt-Co/RGO-ST (77.6%, entry 6) was also higher than that over monometallic Pt/RGO-MW (42.1%, entry 3), which indicates that the addition of Co to Pt can improve the selective activation of C=O and that the Pt_3Co alloy was extremely selective toward the formation of COL. The calculated specific activity of each Pt atom in Pt_3Co/RGO-MW reached 23.8 min^{-1}, and this is 2.7 and 2.4 times that in Pt_3Co/RGO-IM and Pt-Co/RGO-ST (8.8 and 10.0 min^{-1}), respectively. The activity of Pt_3Co/RGO-MW is better than that of Pt-Co/CNTs and Pt-Co/graphite [45]. These results suggest that the RGO sheets pretreated under microwave irradiation contain less oxygen species and are relatively less dense in terms of packing and that they are well exfoliated. This might promote the accessibility of active sites and reactants. Additionally, the proportion of Pt(0) in Pt_3Co/RGO-MW is higher than that in Pt-Co/RGO-ST and Pt_3Co/RGO-IM, which is favorable for the hydrogenation reaction.

Table 3
Catalytic results for the hydrogenation of cinnamaldehyde.

Entry	Catalyst	Conversion (%)	Selectivity (%)			TOF [a] (min^{-1})
			HCAL	HCOL	COL	
1	RGO-MW	<1	—	—	—	—
2	Co/RGO-MW	<1	—	—	—	—
3	Pt/RGO-MW	92.6	40.3	17.6	42.1	21.5
4	Pt_3Co/RGO-MW	99.7	2.5	2.2	95.3	23.8
5	Pt_3Co/RGO-IM	53.6	7.8	0.0	92.2	8.8
6	Pt-Co/RGO-ST	66.6	20.7	1.7	77.6	10.0

Reaction conditions: CAL 8.0 mmol, ethanol 20.0 mL, S/C = 1127, H_2 2.0 MPa, 70 °C, 90 min.

[a] TOF was defined as (the amount of converted CAL molecular at 20 min)/(total amount of Pt atom)/(reaction time, min).

Fig. 7(a) shows the time course of hydrogenation of CAL over Pt_3Co/RGO-MW. The conversion of CAL increased quickly to 90% in the first 60 min and further increased to 99.7% at 90 min. The selectivity toward COL remained higher than 90% even upon the complete conversion of CAL (at 120 min). The formation rate of HCOL was lower than that over Pt/RGO-MW (Fig. 7(b)). These results further confirm that the Pt_3Co alloy was selective toward the formation of COL during the complete conversion of CAL. We also found excellent performance for the selective formation of COL on the Pt_3Co alloy over the time course for Pt_3Co/RGO-IM (Fig. 7(c)). The selectivity toward COL remained higher than 87.0%. However, the selectivity

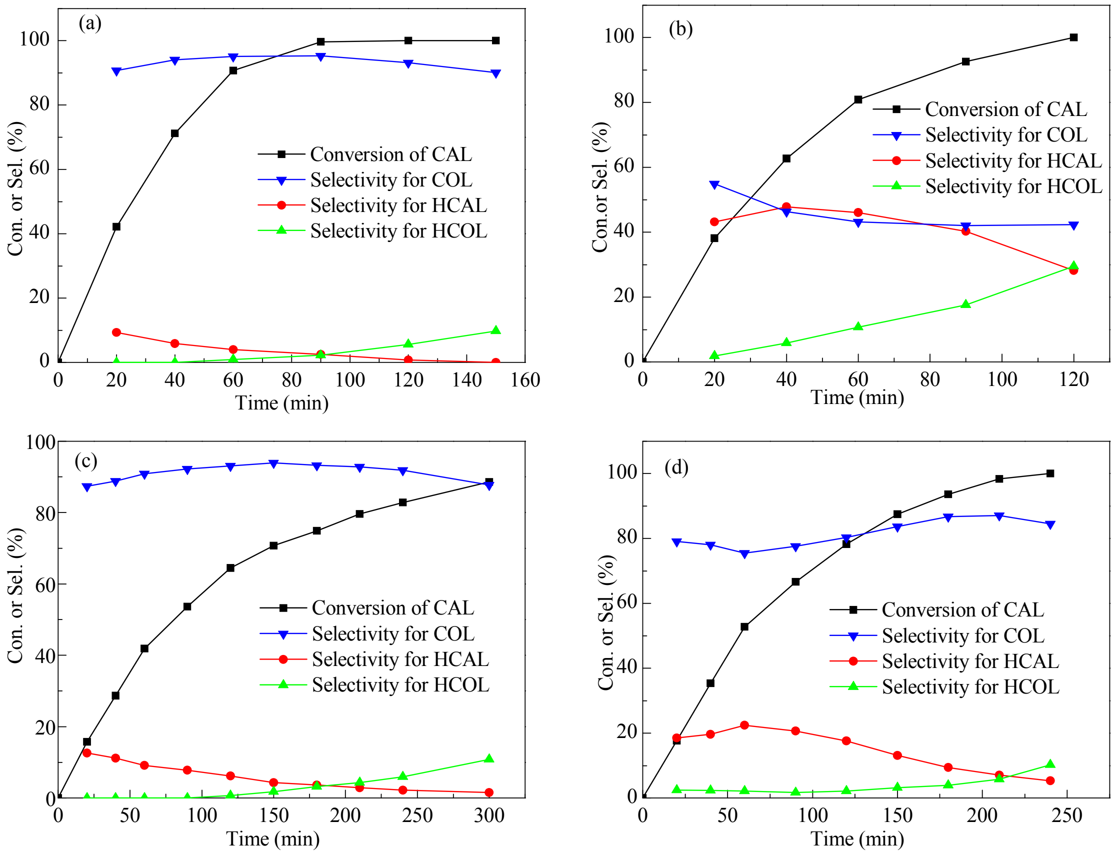

Fig. 7. Time course of CAL hydrogenation over the Pt_3Co/RGO-MW (a), Pt/RGO-MW (b), Pt_3Co/RGO-IM (c) and Pt-Co/RGO-ST (d).

toward COL over Pt-Co/RGO-ST decreased to 77.6% because of the low Co content of the Pt-Co alloy (Fig. 7(d)). Pt_3Co/RGO-MW recycling experiments were also conducted and the results are shown in Fig. 8. We found that the Pt_3Co/RGO-MW catalyst still had good activity after five cycles. As shown in Table 4 and Fig. 9, the decreased activity was probably due to minor loss during the recycle. It is important to highlight that the selectivity toward COL remained higher than 83% in these recycle experiments.

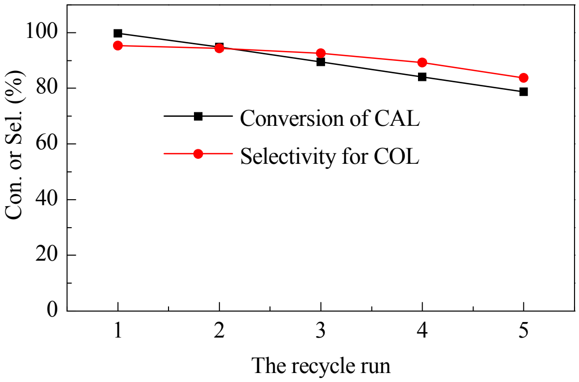

Fig. 8. Recycled Pt_3Co/RGO-MW catalyst during the hydrogenation of CAL.

Table 4
Composition of Pt_3Co/RGO-MW before and after the hydrogenation of CAL.

Catalyst	Metal content [a] (%)		Particle size [b] (nm)
	Pt	Co	
Fresh	15.5	1.6	2.3
Recycled	15.3	1.6	3.1

[a] Analyzed by ICP–AES; [b] Measured by TEM.

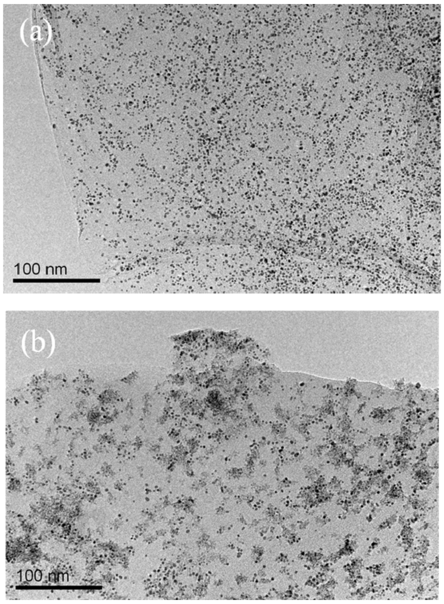

Fig. 9. TEM images of fresh (a) and used (b) Pt_3Co/RGO-MW catalyst for 5 recycles.

4. Conclusions

We investigated the convenient and efficient synthesis of homogenously dispersed Pt_3Co alloy NPs on RGO sheets. We found that microwave irradiation heating is important for the high utilization of Pt and Co precursors. The atomic ratio was easily controlled compared with impregnation and sol-vent-thermal methods. Additionally, microwave irradiation heating prevented the re-graphitization of graphene sheets. In the hydrogenation of CAL, the Pt_3Co/RGO-MW was extremely active and selective toward COL.

References

[1] Tian N, Zhou Z Y, Sun S G, Ding Y, Wang Z L. *Science*, 2007, 316: 732
[2] Stamenkovic V R, Mun B S, Arenz M, Mayrhofer K J J, Lucas C A, Wang G F, Ross P N, Markovic N M. *Nat Mater*, 2007, 6: 241
[3] Ghosh T, Leonard B M, Zhou Q, DiSalvo F J. *Chem Mater*, 2010, 22: 2190
[4] Jusys Z, Behm R J. *J Phys Chem B*, 2001, 105: 10874
[5] Lee A F, Gee J J, Theyers H J. *Green Chem*, 2000, 2: 279
[6] Nie R F, Liang D, Shen L, Gao J, Chen P, Hou Z Y. *Appl Catal B*, 2012, 127: 212
[7] Liang D, Gao J, Sun H, Chen P, Hou Z Y, Zheng X M. *Appl Catal B*, 2011, 106: 423
[8] Tsang S C, Cailuo N, Oduro W, Kong A T S, Clifton L, Yu K M K, Thiebaut B, Cookson J, Bishop P. *ACS Nano*, 2008, 2: 2547
[9] Shi J J, Nie R F, Chen P, Hou Z Y. *Catal Commun*, 2013, 41: 101
[10] Vu H, Gonçalves F, Philippe R, Lamouroux E, Corrias M, Kihn Y, Plee D, Kalck P, Serp P. *J Catal*, 2006, 240: 18
[11] Yang H Z, Zhang J, Sun K, Zou S Z, Fang J Y. *Angew Chem Int Ed*, 2010, 49: 6848
[12] Choi S I, Choi R, Han S W, Park J T. *Chem-Eur J*, 2011, 17: 12280
[13] Wang C, Wang G F, van der Vliet D, Chang K C, Markovic N M, Stamenkovic V R. *Phys Chem Chem Phys*, 2010, 12: 6933
[14] Callejas-Tovar R, Liao W T, de la Hoz J M M, Balbuena P B. *J Phys Chem C*, 2011, 115: 4104
[15] Wu B H, Huang H Q, Yang J, Zheng N F, Fu G. *Angew Chem Int Ed*, 2012, 51: 3440
[16] Kwon S G, Krylova G, Sumer A, Schwartz M M, Bunel E E, Marshall C L, Chattopadhyay S, Lee B, Jellinek J, Shevchenko E V. *Nano Lett*, 2012, 12: 5382
[17] Shao Y Y, Zhang S, Wang C M, Nie Z M, Liu J, Wang Y, Lin Y H. *J Power Sources*, 2010, 195: 4600
[18] Guo S J, Dong S J, Wang E K. *ACS Nano*, 2010, 4: 547
[19] Kundu P, Nethravathi C, Deshpande P A, Rajamathi M, Madras G, Ravishankar N. *Chem Mater*, 2011, 23: 2772
[20] Bock C, Paquet C, Couillard M, Botton G A, MacDougall B R. *J Am Chem Soc*, 2004,126: 8028
[21] Santori G F, Casella M L, Ferretti O A. *J Mol Catal A*, 2002, 186: 223
[22] Yue Q L, Zhang K, Chen X M, Wang L, Zhao J S, Liu J F, Jia J B. *Chem Commun*, 2010, 46: 3369
[23] Scheuermann G M, Rumi L, Steurer P, Bannwarth W, Mülhaupt R. *J Am Chem Soc*, 2009, 131: 8262
[24] Nie R F, Wang J H, Wang L N, Qin Y, Chen P, Hou Z Y. *Carbon*, 2012, 50: 586
[25] Siamaki A R, Khder A E R S, Abdelsayed V, El-Shall M S, Gupton B F. *J Catal*, 2011, 279: 1
[26] Zhao Y C, Zhan L, Tian J N, Nie S L, Ning Z. *Electrochim Acta*, 2011, 56: 1967
[27] Verma S, Mungse H P, Kumar N, Choudhary S, Jain S L, Sain B, Khatri O P. *Chem Commun*, 2011, 47: 12673
[28] Allen M J, Tung V C, Kaner R B. *Chem Rev*, 2010, 110: 132
[29] Si Y C, Samulski E T. *Chem Mater*, 2008, 20: 6792
[30] Chen S Q, Wang Y. *J Mater Chem*, 2010, 20: 9735
[31] Hu H, Zhao Z B, Zhou Q, Gogotsi Y, Qiu J S. *Carbon*, 2012, 50: 3267
[32] Knupp S L, Li W Z, Paschos O, Murray T M, Snyder J, Haldar P. *Carbon*, 2008, 46: 1276
[33] Jiang S J, Ma Y W, Jian G Q, Tao H S, Wang X Z, Fan Y N, Lu Y N, Hu Z, Chen Y. *Adv Mater*, 2009, 21: 4953
[34] Yu W Y, Tu W X, Liu H F. *Langmuir*, 1999, 15: 6
[35] Hummers W S Jr, Offemann R E. *J Am Chem Soc*, 1958, 80: 1339
[36] Fei L F, Sun T Y, Lu W, An X Q, Hu Z F, Yu J C, Zheng R K, Li X M, Chan H L W, Wang Y. *Chem Commun*, 2014, 50: 826
[37] Li X L, Zhang G Y, Bai X D, Sun X M, Wang X R, Wang E G, Dai H J. *Nat Nanotechnol*, 2008, 3: 538
[38] Chen J L, Yan X P. *J Mater Chem*, 2010, 20: 4328

Graphical Abstract

Chin. J. Catal., 2014, 35: 2029–2037 doi: 10.1016/S1872-2067(14)60232-1

Microwave assisted fast fabrication of nanosized Pt_3Co alloy on reduced graphene oxides

Juanjuan Shi, Renfeng Nie, Mengyuan Zhang, Mengsi Zhao, Zhaoyin Hou*
Zhejiang University

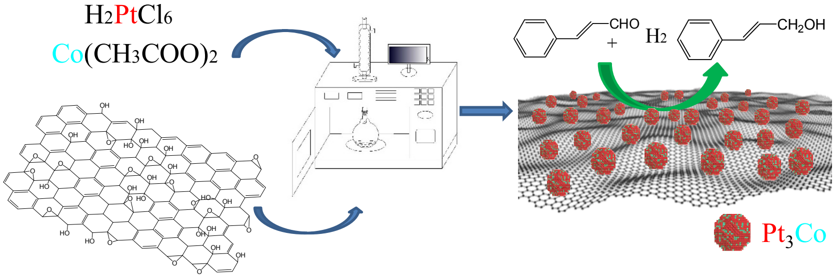

A microwave irradiation-prepared nanosized Pt_3Co alloy was supported on reduced graphene oxides and the synthesized Pt_3Co/RGO-MW was used for the selective hydrogenation of cinnamaldehyde to cinnamyl alcohol.

[39] Pimenta M A, Dresselhaus G, Dresselhaus M S, Cançado L G, Jorio A, Saito R. *Phys Chem Chem Phys*, 2007, 9: 1276

[40] Paredes J I, Villar-Rodil S, Solís-Fernández P, Martínez-Alonso A, Tascón J M D. *Langmuir*, 2009, 25: 5957

[41] Vinayan B P, Ramaprabhu S. *Nanoscale*, 2013, 5: 5109

[42] Liang Y M, Zhang H M, Zhong H X, Zhu X B, Tian Z Q, Xu D Y, Yi B L. *J Catal*, 2006, 238: 468

[43] Gao C L, Liang Y Y, Han M, Xu Z, Zhu J M. *J Phys Chem C*, 2008, 112: 9272

[44] Duong H T, Rigsby M A, Zhou W P, Wieckowski A. *J Phys Chem C*, 2007, 111: 13460

[45] Li Y, Zhu P F, Zhou R X. *Appl Surf Sci*, 2008, 254: 2609